J. E. Purkinje University in Ústí nad Labem
Faculty of Science
Department of Physics

Abstract of the Doctoral Thesis

Self-Assembly in Diblock Copolymer Systems: Insight from Dissipative Particle Dynamics

Author:

Zbyšek Posel

Supervisor:

Martin Lísal

Ústí nad Labem, 2012

UNIVERZITA J. E. PURKYNĚ V ÚSTÍ NAD LABEM
PŘÍRODOVĚDECKÁ FAKULTA
KATEDRA FYZIKY

AUTOREFERÁT DISERTAČNÍ PRÁCE

DISIPATIVNÍ ČÁSTICOVÁ DYNAMIKA SAMOORGANIZACE DIBLOKOVÝCH KOPOLYMERŮ

Autor:
ZBYŠEK POSEL

Školitel:
MARTIN LÍSAL

Ústí nad Labem, 2012

Disertační práce byla vypracována na základě vědeckých výsledků na katedře fyziky Přírodovědecké fakulty Univerzity J. E. Purkyně v Ústí nad Labem v letech 2008-2013 v rámci doktorského studia P1703 Počítačové metody ve vědě a technice.

Doktorand: Mgr. Zbyšek Posel

Školitel: Doc. Ing. Martin Lísal, DSc.
Katedra fyziky, PřF UJEP
České Mládeže 8, 400 96 Ústí nad Labem;
Ústav chemických procesů AV ČR, v. v. i.
Rozvojová 135, 165 02 Praha 6 - Suchdol

Oponenti: Doc. Ing. Zuzana Limpouchová, CSc
Katedra fyzikální a makromolekulární chemie, PřF UK
Hlavova 2030/8, 128 43 Praha 2

Dr. Flor R. Siperstein
School of Chemical Engineering and Analytical Science
The University of Manchester, Manchester M13 9PL, UK

Autoreferát byl odeslán dne:
Ke stažení je na adrese http://sci.ujep.cz/doktorskestudium-info.html.

Obhajoba se koná dne v hodin před komisí pro obhajoby disertačních prací v oboru P1703 Počítačové metody ve vědě a technice na Přírodovědecké fakultě Univerzity J. E. Purkyně v Ústí nad Labem, místnost , České Mládeže 8, 400 96 Ústí nad Labem.

S disertací je možno se seznámit na studijním oddělení Přírodovědecké fakulty Univerzity J. E. Purkyně v Ústí nad Labem.

Předseda OR: prof. RNDr. Rudolf Hrach, DrSc.
Katedra fyziky, PřF UJEP
České Mládeže 8, 400 96 Ústí nad Labem

[44] A. J. Schultz, C. K. Hall, J. Genzer, J. Chem. Phys. 2004, 120, 2049-2055.

[45] T. L. Morkved, P. Štěpánek, K. Krishnan, F. S. Bates, T. P. Lodge, J. Chem. Phys. 2001, 114, 7247-7259.

[46] K. Krishnan, F. S. Bates, T. P. Lodge, J. Rheol. 2005, 49, 1395-1408.

[47] D. J. Norris, A. L. Efros, S. C. Erwin, Science 2008, 319, 1776-1779.

[48] M. Grzelczak, J. Vermant, E. M. Furst, L. M. Liz-Marzán, ACS Nano 2010, 4, 3591-3605.

[49] H.-C. Kim, S.-M. Park, W. D. Hinsberg, Chem. Rev. 2010, 110, 146-177.

[50] K. M. Langner, G. J. A. Sevink, Soft Matt. 2012, 8, 5102-5118.

[30] J. A. Millan, W. Jiang, M. Laradji, Y. Wang, J. Chem. Phys. 2007, 126, 124905-124914.

[31] S. Chen, N. Phan-Thien, X.-J. Fan, B. C. Khoo, J. Non-Newtonian Fluid Mech. 2004, 118, 65-81.

[32] J. Huang, M. Luo, Y. Wang, J. Phys. Chem. B 2008, 112, 6735-6741.

[33] D. Reith, M. Pütz, F. Müller-Plathe, J. Comput. Chem. 2003, 24, 1624-1636.

[34] N. Chennamsetty, H. Bock, M. Lísal, J. K. Brennan, in *Process Systems Engineering, Volume 6: Molecular Systems Engineering* (edited by C. S. Adjiman and A. Galindo, WILEY-VCH, Weinheim, Germany, 2010).

[35] C. Tzoumanekas, F. Lahmar, B. Rousseau, D. N. Theodorou, Macromolecules 2009, 42, 7474-7484.

[36] F. Lahmar, C. Tzoumanekas, D. N. Theodorou, B. Rousseau, Macromolecules 2009, 42, 7485-7494.

[37] N. Ch. Karayiannis, A. E. Giannousaki, V. G. Mavrantzas, D. N. Theodorou, J. Chem. Phys. 2002, 117, 5465-5479.

[38] R. G. Larson, Macromolecules 1994, 27, 4198-4203.

[39] Q. Wang, Q. Yan, P. F. Nealey, J. J. de Pablo, J. Chem. Phys. 2000, 112, 450-464.

[40] T. M. Beardsley, M. W. Matsen, Europhys. J. E 2010, 32, 255-264.

[41] M. Murat, G. S. Grest, K. Kremer, Macromolecules 1999, 32, 595-609.

[42] W. H. Press, B. P. Flannery, S. A. Teukolsky, W. T. Vetterling, *Numerical Recipes. The Art of Scientific Computing* (University Press, Cambridge, 1990).

[43] A. J. Schultz, C. K. Hall, J. Genzer, J. Chem. Phys. 2002, 117, 10329-10338.

Table of Contents

Abstract of the Thesis

The general goals of the thesis is application of mesoscale modeling on the rich phase behavior of the diblock copolymer-homopolymers systems and systems of diblock copolymers with embedded nanoparticles. At first, the thesis deals with conformational and dynamic behavior of coarse-grained polymer models. Three homopolymer models are investigated and the results are compared with predictions given by the Rouse theory which is considered as a standard theory for unentangled polymer melts. Then technical aspects of simulations of lamellar morphology are investigated. The incommensurability of simulation box size and lamellar morphology is demonstrated on determination of the lamellar spacing for generally oriented lamellar planes. The thesis then focuses on microphase behavior of lamellae forming diblock copolymer-homopolymers systems. The phase behavior, i.e., the phase boundaries between the disordered and lamellar regions and between the disordered and two phase regions, were predicted for the real diblock copolymer-homopolymers melt of poly(ethylethylene) and poly(dimethylsiloxane) homopolymers and corresponding poly(ethylethylene)-poly(dimethylsiloxane) diblock copolymer. Finally, the thesis focuses on the systems based on poly(styrene-*b*-2-vinylpyridine) (PS-PVP) diblock copolymers in which the gold nanoparticles, grafted with a mixture of PS/PVP homoligands, are dispersed. The effect of nanoparticle's volume fraction and decoration, and of the diblock copolymer architecture on morphology of nanocomposites is presented in phase diagrams. The predicted behavior of the nanocomposites is in agreement with experimental evidence on the same or similar related systems.

[14] J. Y. Lee, R. B. Thompson, D. Jasnow, A. C. Balazs, Macromolecules 2002, 35, 4855-4858.

[15] R. B. Thompson, V. V. Ginzburg, M. W. Matsen, A. C. Balasz, Macromolecules 2002, 35, 1060-1071.

[16] A. R. Leach, *Molecullar Modelling. Principles and Applications* (2^{nd} Ed., Pearson Education Limited, 2001).

[17] P. J. Hoogerbrugge, J. M. V. A. Koelman, Europhys. Lett. 1992, 19, 155-160.

[18] R. D. Groot, P. B. Warren, J. Chem. Phys. 1997, 107, 4423-4435.

[19] R. D. Groot, T. J. Madden, J. Chem. Phys. 1998, 108, 8713-8724.

[20] F. Lahmar, B. Rousseau, Polymer 2007, 48, 3584-3592.

[21] C.-I. Huang, L.-F. Yang, C.-H. Lin, H.-T. Yu, Theory Simul. 2008, 17, 198-207.

[22] M. Lísal, J. K. Brennan, Langmuir 2007, 23, 4809-4818.

[23] P. Petrus, M. Lísal, J. K. Brennan, Langmuir 2010, 26, 3695-3709.

[24] P. Petrus, M. Lísal, J. K. Brennan, Langmuir 2010, 26, 14680-14693.

[25] M. Malý, P. Posocco, S. Pricl, M. Fermeglia, Ind. Eng. Chem. Res. 2008, 47, 5023-5038.

[26] P. Posocco, Z. Posel, M. Fermeglia, M. Lísal, S. Pricl, J. Mater. Chem. 2010, 20, 10511-10520.

[27] N. A. Spenley, Europhys. Lett. 2000, 49, 534-540.

[28] M. Doi, S. F. Edwards, *The Theory of Polymer Dynamics* (5^{th} Ed., Calderon Press, Oxford, 1994).

[29] Y.-H. Wu, D.-M. Wang, J.-Y. Lai, J. Phys. Chem. B 2008, 112, 4604-4612.

Reference

[1] A. J. Meuler, M. A. Hillmyer, F. Bates, Macromolecules 2009, 42, 7221-7250.

[2] A. K. Khandpur, S. Förster, F. S. Bates, I. W. Hamley, A. J. Ryan, W. Bras, K. Almdal, K. Mortensen, Macromolecules 1995, 28, 8796-8806.

[3] T. Inoue, T. Soen, T. Hashimoto, H. Kawai, J. Polym. Sci. Polym. Phys. 1969, 7, 1283-1301.

[4] M. Gervais, B. Gallot, Macromol. Chem. 1973, 171, 157-178.

[5] T. Hashimoto, K. Nagatoshi, A. Todo, H. Hasegawa, H. Kawai, Macromolecules 1974, 7, 364-373.

[6] D. A. Hajduk, P. E. Harper, S. M. Gruner, Ch. C. Honecker, G. Kim, E. L. Thomas, Macromolecules 1994, 27, 4063-4075.

[7] E. W. Cochran, C. J. Garcia-Cervera, G. H. Frederickson, Macromolecules 2006, 39, 2449-2451.

[8] G. H. Fredrickson, F. S. Bates, Annu. Rev. Mat. Sci. 1996, 26, 501-550.

[9] G. M. McClelland, M. W. Hart, C. T. Rettner, M. E. Best, K. R. Carter, B. D. Terris, Appl. Phys. Lett. 2002, 81, 1483-1485.

[10] M. P. Stoykovich, M. Muller, S. O. Kim, H. H. Solak, E. W. Edwards, J. J. de Pablo, P. F. Nealey, Science 2005, 308, 1442-1446.

[11] H. L. Rosano, M. Clause, *Microemulsion Systems* (1st Ed., CRC Press, 1987).

[12] F. S. Bates, W. W. Maurer, P. M. Lipic, M. A. Hillmyer, K. Almdal, K. Mortensen, G. H. Fredrickson, T. P. Lodge, Phys. Rev. Lett. 1997, 79, 849-852.

[13] R. B. Thompson, V. V. Ginzburg, M. W. Matsen, A. C. Balasz, Science 2001, 292, 2469-2472.

Abstrakt disertační práce

Předkládaná práce popisuje pomocí mesoskopických simulací komplexní fázové chování diblokových kopolymerů s homopolymery a diblokových kopolymerů s nanočásticemi. Práce se nejprve zabývá strukturními a dynamickými vlastnostmi tří hrubozrnných polymerních modelů. Výsledky jsou porovnány s Rouseho teorií, která představuje základní teorii pro popis polymerní taveniny. Dále je v práci studován vliv nesouměřitelnosti simulačního boxu a lamelární struktury na výslednou šířku lamely, získanou pomocí mesoskopických simulací. Komplexní fázové chování diblokových kopolymerů s homopolymery je studováno pomocí mesoskopických simulací pro homopolymery poly(dimethylsiloxanu) (PDMS) a poly(ethylethylenu) (PEE) a diblokové kopolymery PDMS-PEE tvořící lamely. Na základě výsledků simulací jsou stanoveny hranice mezi neuspořádaným stavem a lamelární oblastí a mezi neuspořádaným stavem a dvou fázovou oblastí. Nakonec práce pomocí mesoskopických simulací popisuje chování nanokompozitů složených z diblokových kopolymerů poly(styrenu-*b*-2-vinylpyridinu) (PS-PVP) a nanočástic zlata, které jsou pokryty směsí PS/PVP homopolymerů. Vliv množství nanočástic, jejich pokrytí a struktury diblokového kopolymeru na výsledné nanokompozity je popsán pomocí fázových diagramů. Výsledné fázové chování nanokompozitů z mesoskopických simulací se shoduje s experimentálním popisem reálných systémů.

1 Introduction

In the last two decades, diblock copolymers (DBCs) have been extensively studied by experiment and theory [1,2]. The DBCs are composed of two chemically incompatible homopolymers that are covalently bonded. They are able to self-assemble into four periodically ordered nanostructures that minimize contacts between the two homopolymers; namely: lamellae, hexagonally packed cylinders, spheres ordered to body-center-cubic lattice [3–5], and a gyroid phase [6, 7].

Dynamics of the DBC nanostructures as well as their static properties are now well described [8] and DBCs are widely used in various applications such as enhancement of computer memory, nanoscale templating or nanoscale separations [9,10], just to mention a few. Nevertheless increase of industrial interest in further applications of advanced materials as well as in design and manufacture of tailor-made materials has indicated that pure DBC systems cannot satisfy all practical demands and more complex systems such as mixtures and melts of the DBCs with another compounds are required. Among plethora of systems and their possible applications two systems are of special interest: (i) ternary melts of DBC with additional two incompatible homopolymers and (ii) DBCs with embedded inorganic nanoparticles (NPs). The former systems have ability to stabilize a bicontinuous microemulsion (BμE) phase [11, 12] while in the latter systems, the embedded NPs enhance DBC features and affect the DBC morphologies [13–15].

The properties and morphology of the DBC-homopolymers and nanocomposite systems are influenced by a large number of parameters. It is impractical to explore effects of these parameters solely by experimental techniques, and therefore, theoretical approaches along with computer simulations are employed to complement the experiments. Computer simulations [16] can describe, depending on models employed, a detailed molecular-level picture of system structures as well as hydrodynamics of microphase separations.

The time and length scales of the dynamic processes corresponding to the relevant material properties of the DBC-homopolymers and nanocomposite systems are beyond the limit of atomistic modeling and simulations of these systems rely on coarse-grain models that retain only the most

5 Papers Included in the Thesis

The following results were or will be published based on the results of the thesis.

[P1] **Z. Posel**, M. Lísal, J. K. Brennan: Interplay between microscopic and macroscopic phase separations in ternary polymer melts: Insight from mesoscale modelling. Fluid Phase Equilib. 2009, 283, 38-48. **IF 2.14**

[P2] P. Posocco, **Z. Posel**, M. Fermeglia, M. Lísal, S. Pricl: A molecular simulation approach to the prediction of the morphology of self-assembled nanoparticles in diblock copolymers. J. Mater. Chem. 2010, 20, 10511-10520. **IF 5.1**

[P3] **Z. Posel**, P. Posocco, M. Fermeglia, M. Lísal, S. Pricl: Modeling hierarchically structured nanoparticle/diblock copolymer systems. Soft Matt. 2012, DOI: 10.1039/c2sm27360h. **IF 4.39**

[P4] **Z. Posel**, B. Rousseau, M. Lísal: Scaling behavior of different polymer models in dissipative particle dynamics of unentangled melts. Molec. Phys. 2013, to be submitted. **IF 1.82**

[P5] **Z. Posel**, J. Škvor: Simulation aspects of lamellar morphology: Incommensurability effect. Macromol. Theory Simul. 2013, submitted. **IF 1.71**

of the coarse-graining procedure employed, the experimental boundaries between the disordered and lamellar regions, and between the disordered and two-phase regions were predicted quite well by DPD models.

Fourth, we systematically studied the effect of nanoparticles location on the morphology of nanocomposites on a model system of poly(styrene-*b*-2-vinylpyridine) (PS-*b*-PVP) and gold nanoparticles decorated by oligomeric chains of PS and PVP. We predicted the effects of nanoparticle volume fraction, surface chemistry and diblock copolymer architecture on morphologies of nanocomposite are in agreement with experimental evidence on the same or similar related systems. Our results further confirmed that the morphologies of organic/inorganic hybrid materials can be tailored by adding nanoparticles of specific size and chemistry. Finally, the results also highlighted that in complex systems such as nanocomposites, the ordering of the diblock copolymers does not simply template the spatial organization of the nanoparticles; the nanoparticle concentration is not a ”passive scalar” and can affect the self-assembly of the diblock copolymer chains.

essential features of the system species. Hoogerbrugge and Koelman [17] introduced a mesoscale technique to simulate hydrodynamic behavior, called dissipative particle dynamics (DPD). DPD is a computational tool for simulating Newtonian and non-Newtonian fluids, including polymer systems [18, 19], on mesoscopic length and time scales. Presently for polymer systems, DPD has been used to simulate static and dynamic properties of polymer melts [20], self-assembly of DBCs in bulk [21], under shear [22] and in confinement [23, 24], and self-assembly of NPs in DBCs [25, 26], just to mention a few.

2 Aims of the Thesis

The general goal of the thesis is application of mesoscale simulations on the rich microphase behavior of the diblock copolymer-homopolymers systems and systems of diblock copolymers with embedded inorganic nanoparticles. The thesis first deals with conformational and dynamic behavior of coarse-grain polymer models and technical aspects of simulation of the lamellar morphology. Then, the thesis focuses on microphase behavior of the lamellae forming diblock copolymer-homopolymers systems and on the systems based on PS-*b*-PVP diblock copolymers in which the gold nanoparticles grafted with a mixture of PS and PVP short homoligands are dispersed.

The problems addressed in the thesis have been a part of a long-term research conducted in Department of Physics, Faculty of Science, J. E. Purkinje University, in E. Hála Laboratory of Thermodynamics, Institute of Chemical Process Fundamentals of the ASCR, v. v. i., and in the collaborating Molecular Simulations Engineering Laboratory, Department of Engineering and Architecture, University of Trieste, Italy. The research was supported by the European Community under the 6th Framework Programme (Project MULTIPRO No. 033304) and under the 7th Framework Programme (Project COST No. TD0802) and by the Internal Grant Agency of the J. E. Purkinje University.

4 Conclusions

The thesis used dissipative particle dynamics (DPD), mesoscopic simulation technique, to explore the microphase behavior of the diblock copolymer-homopolymers systems and systems of diblock copolymers with embedded inorganic nanoparticles.

First, we studied the scaling behavior for the conformational and dynamic properties of three coarse-grain polymer models typically employed in DPD simulations of unentangled polymer melts. The scaling behavior of the first model followed the Rouse model exactly for the chain lengths greater than about 20. The second model used FENE spring equivalent to harmonic spring of the first model and we found that its scaling behavior was identical to that of the first model. The third model represented a real polyethylene at mesoscale and unlike the first and second polymer models, it exhibited a bending stiffness. The third model with more than ten mesoscopic beads obeyed the Rouse scaling exactly for the conformational properties and also rather well for the center-of-mass self-diffusion coefficient. The increase of the viscosity with the chain length was found to be rather different than that predicted by the Rouse theory.

Second, we studied the effects of the box size on the lamellar structure of diblock copolymer melts. We determined the natural lamellar spacing, which corresponds to a lamellar width of a lamellar structure with the lowest free energy, by varying the box lengths at fixed system volume and equalizing the pressure in each direction. We found that for various system volumes and lamellar orientations this approach resulted in the same value of the natural lamellar spacing.

Third, we predicted the phase diagram of ternary polymer melts comprising of low molecular weight poly(dimethyl siloxane) (PDMS) and poly(ethyl ethylene) (PEE) homopolymers, and a nearly symmetric PDMS-PEE diblock copolymer. In contrast to the experimental phase diagram of the PDMS/PEE/PDMS-PEE melt that shows disordered, lamellar, bicontinuous microemulsion and multi-phase regions, the mesoscale model phase diagrams only displayed disordered, lamellar, and two-phase regions with a Lifshitz point located at concentrations where the experimental phase diagram exhibits a narrow channel of bicontinuous microemulsion. Despite the simplicity

the highest values of V_f and PVP coverage of NPs. On the other hand, spherical and cylindrical morphologies are affected by increasing NP concentration and change in PS/PVP coverage of NPs, although in a different extent.

Thus, when the NPs are entirely decorated by the PS chains (Fig. 6a), the cylindrical morphology is predicted to be the only morphology subject to the influence of the NP concentration. As expected for all systems, the NPs are located inside the corresponding PS domain. This, in turn, results in an alteration of the corresponding underlying ordered structure as V_f increases. The reason why for the system with PS_6-PVP_{14} ($f = 0.3$), a rather larger number of NPs can be accommodated in the cylindrical domains without inducing detectable defects is found in the larger value of cylinder diameters with respect to the other systems with cylindrical morphologies, PS_4-PVP_{16} ($f = 0.2$) and PS_5-PVP_{15} ($f = 0.25$).

As the PVP coverage of NPs increases, a dramatic effect is observed: the presence of even a very small amount of PVP on the NP surface is sufficient to suppress a change in morphology for the system with PS_4-PVP_{16} ($f = 0.2$) up to $V_f = 0.1$ (Fig. 6b) while a further increase in the PVP coverage of NPs helps to stabilize the cylindrical phase in the systems PS_4-PVP_{16} ($f = 0.2$) and PS_5-PVP_{15} ($f = 0.25$), again up to high values of V_f.

Finally, in the systems with PS_8-PVP_{12} ($f = 0.4$) and PS_{10}-PVP_{10} ($f = 0.5$) no change in the lamellar morphology was detected over the entire range of V_f studied. However, in the system with PS_8-PVP_{12} ($f = 0.4$), for NPs with a high PVP coverage and at $V_f = 0.1$, NPs aggregation was observed which ultimately led to perforation of lamellae and extravasation of the NPs into the PS domain (Figs. 6e-g). Interestingly, analogous behavior is not predicted for the lamellar phase in the system with PS_{10}-PVP_{10} ($f = 0.5$). Such the difference is related to the thickness of lamellae: in the case of PS_8-PVP_{10} ($f = 0.4$), the PS domain is thinner than the PVP domain and upon aggregation of the NPs within the PVP domain, the lamellar interface breaks and NPs can easily penetrate into the PS domain.

3 Results

3.1 Conformation and Dynamics of Coarse-Grain Polymers

Generally, real polymers in melts and solutions are known to follow a number of scaling laws, i.e., their conformational and dynamic properties such the end-to-end distance or viscosity scale with the chain length N. A coarse-grain polymer model should reproduce scaling laws in order the model can be considered as a reliable mesoscopic representation of a real polymer. Spenley [27] has shown that the scaling laws for the Groot and Warren [18] (GW) model, traditionally used in DPD, are in excellent agreement with the scaling laws predicted by the Rouse theory which is consider as a standard theory for unentangled polymer melts [28]. However, a large variety of problems tackled by DPD simulations led to employing polymer models that differ from the original GW model [18], e.g., models with stiff harmonic springs [29], models with a finitely extensible nonlinear elastic (FENE) spring instead of the harmonic spring [30–32], and models with bead-bead and intramolecular potentials derived by the IBI approach [33, 34]. For such the models, the scaling laws have not been explored yet. Motivated by the polymer models beyond the original GW model, we systematically explored scaling laws for the conformational and dynamic properties of three coarse-grain polymer models often used in DPD below the critical polymer mass.

Model 1 corresponds to the GW model but with increased chain stiffness K_H^*. The DPD simulations were performed for $K_H^* = \{2, 4, 6, 10\}$ where $K_H^* = 2$ corresponds to the GW model [18] studied by Spenley [27]. By plotting the simulation results in logarithmic scale, we observed that the conformational and dynamic properties scale linearly with the chain length only for large N and they show a weak departure from the linearity at small N. The ratio $\mathcal{R}$ of squared end-to-end distance R_e^{*2} and squared radius of gyration R_g^{*2}, shown in Fig. 1a, clearly indicates two scaling regimes. For $N > (20 - 30)$, $\mathcal{R}$ is almost constant and is close to unity as predicted by the Rouse theory. For $N < 20$, $\mathcal{R}$ becomes less than one and decreases with shortening of polymer chains. Figs. 1b and 1c then compare the simulation values of R_e^* and R_g^*

with the predictions from the Rouse theory. We see that the simulated R_e^* agrees quite well with the Rouse scaling even at small N, except the simulated R_e^* for $K_H^* = 10$ which is below the Rouse predictions. At $N < 10$, the simulated values of R_g^* are higher than the Rouse values. The results for diffusion of center-of-mass of the polymer chain D^* and viscosity η^* (both not shown here) suggest that that D^* is only marginally influenced by the chain stiffness and exhibits rather small deviations only at $N < 10$ and the deviations slightly increase with increasing K_H^*. Unlike for D^*, η^* is strongly influenced by the chain stiffness. Results of the simulated η^* displays rather significant deviations from the Rouse theory at $N < (20 - 30)$ and the deviations are more pronounced for stiffer polymers.

Model 2 was aimed to explore how the conformational and dynamic behavior of the previous polymer model, i.e.Model 1, is influenced by replacement of the harmonic spring with the FENE spring. For Model 2, we thus found equivalent values of FENE spring stiffness K_F^* that corresponds to $K_H^* = \{2, 4, 6, 10\}$. Similarly as for Model 1, we observed two scaling regimes. For $N > (20 - 30)$, Model 2 is in the Rouse regime. The values of simulated $R_e^*(N)$, $R_g^*(N)$, $D^*(N)$ and $\eta^*(N)$ match those of Model 1.

Model 3 is a coarse-grain representation of polyethylene (PE) [35,36]. Due to the presence of the bending stiffness, the PE chains become more stretched than those of Model 1 and Model 2. This is reflected on Flory's characteristic ratio C_N and its asymptotic value, $C_\infty \simeq 1.77$, that is larger than those of Model 1 and Model 2, but still well below the value for real PE, $C_\infty^{\mathrm{PE}} \sim 8$ [37]. Fig. 2 displays the dynamic properties D, ξ and η where the simulation values of ξ for $N > 10$ oscillates around a constant value as assumed in the Rouse theory. Hence for large N, the scaling behavior for D agrees rather well with the Rouse model. For small N, D and equivalently ξ moderately deviate from the Rouse scaling as seen in Figs. 2a and 2b. The results for η (Fig. 2c) also exhibit two distinct scaling regimes: a small increase of η with N for $N < 10$ followed by a sharper increase of η for the larger N. The coarse-grain model of PE thus does not obey the Rouse scaling in the case of the viscosity.

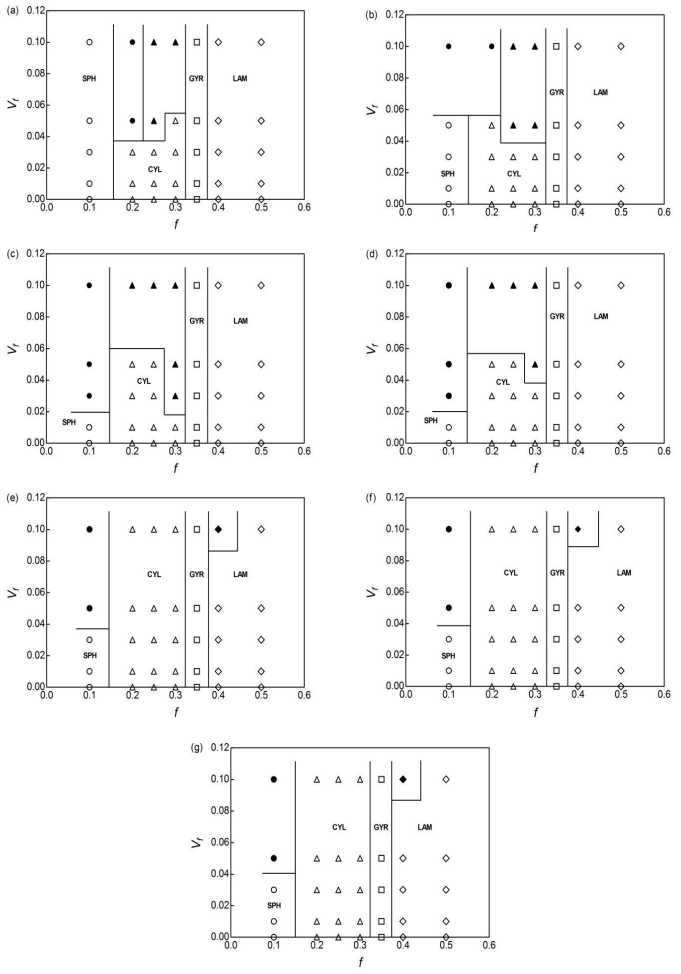

Fig. 6: Phase diagrams of PS-PVP DBCs embedded with gold NPs as a function of the relative DBC composition, f, and NP volume fraction, V_f. NPs were functionalized with a mixture of PS/PVP homoligands in various ratios: (a) PS_{12} ($f_{PS} = 1.0$), (b) $PS_{11}PVP_1$ ($f_{PS} = 0.92$), (c) PS_9PVP_3 ($f_{PS} = 0.75$), (d) PS_6PVP_6 ($f_{PS} = 0.5$), (e) PS_3PVP_9 ($f_{PS} = 0.25$), (f) PS_1PVP_{11} ($f_{PS} = 0.08$), and (g) PVP_{12} ($f_{PS} = 0.0$). Four different DBC morphologies were considered as polymeric matrix: lamellae ($f = 0.5$ and 0.4), gyroid ($f = 0.35$), hexagonally packed cylinders ($f = 0.3, 0.25$ and 0.2), and spheres ($f = 0.1$). Symbols legend: circles, spherical morphology; triangles, cylindrical morphology; squares, gyroid phase; diamonds, lamellar morphology. The empty symbols denote morphologically perfect structures while filled symbols represent morphologically imperfect structures. Lines in phase diagrams are a guide for the eye only.

3.4 Diblock Copolymer-Nanoparticle Systems

Mixing microphase-separating DBCs and NPs leads to the self-assembly of organic/inorganic hybrid materials (nanocomposites) that are spatially organized on the nanometer scale [47, 48]. In order to successfully exploit the self-assembly of the DBC-NP systems in technological applications, and to ensure efficient scale-up, a high level of system spatial ordering is required. Thus, an important goal involved in the engineering of the hybrid materials is attaining precise control of ordered structures and spatial distributions of the polymeric components, NPs, or both. A particularly appealing strategy to avoid NPs aggregation and to selectively incorporate NPs into the preferred domain of DBCs is tailoring the surface chemistry of NPs [49, 50]. In the following, we focused on a system based on a poly(styrene-*b*-2-vinylpyridine) (PS-*b*-PVP) DBC in which functionalized gold NPs were dispersed. NPs were considered grafted with a mixture of short PS and PVP homoligands in different percentages. In our simulations, we systematically varied the relative chain composition f of the DBCs, NP coverage and system volume fraction of NPs V_f, and explored effects of these variables on the system morphology, and dispersion and localization of the NPs in the model nanocomposites. The model mimicked the PS-*b*-PVP DBC with the molecular weight of 21,000 g/mol. Coarse-graining of PS-*b*-PVP DBC was based on atomistic simulations of PS and PVP homopolymers and is described in details in Ref. [25]. The coarse-graining resulted in the chain length $N_{AB} = 20$ where A and B stands for the PS and PVP beads, respectively. A NP was represented by an ensemble of beads arranged in an icosahedral structure. The NP consisted of central Au bead surrounded by 12 beads located at vertices of the icosahedron. The effect of a different NP coverage was modeled by making the icosahedral vertex beads PS- and PVP-like. The volume fraction of the NPs in the system ranged from 1 to 10 % which corresponds to a typical concentration range in practical applications.

The following general features are immediately discernible from Fig. 6. The gyroid phase ($f = 0.35$) and lamellar phase for $f = 0.5$ are predicted to be stable at all NP concentrations and surface grafting compositions. The lamellar phase for $f = 0.4$ seems to be only affected at

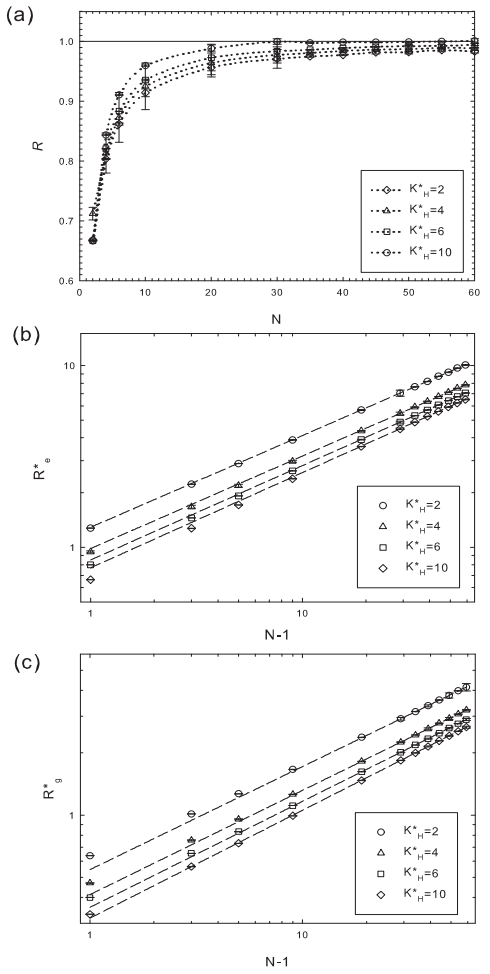

Fig. 1: (a) The ratio $\mathcal{R} = R_e^{*2}/(6R_g^{*2})$, (b) end-to-end distance R_e^*, and (c) radius of gyration R_g^* as a function of the chain length N for Model 1; K_H^* is the harmonic spring constant. The symbols represent simulation results, the dashed lines correspond to fit to $f(N) = A_0 (N-1)^{A_1}$ and dotted lines serve as a guide to the eye.

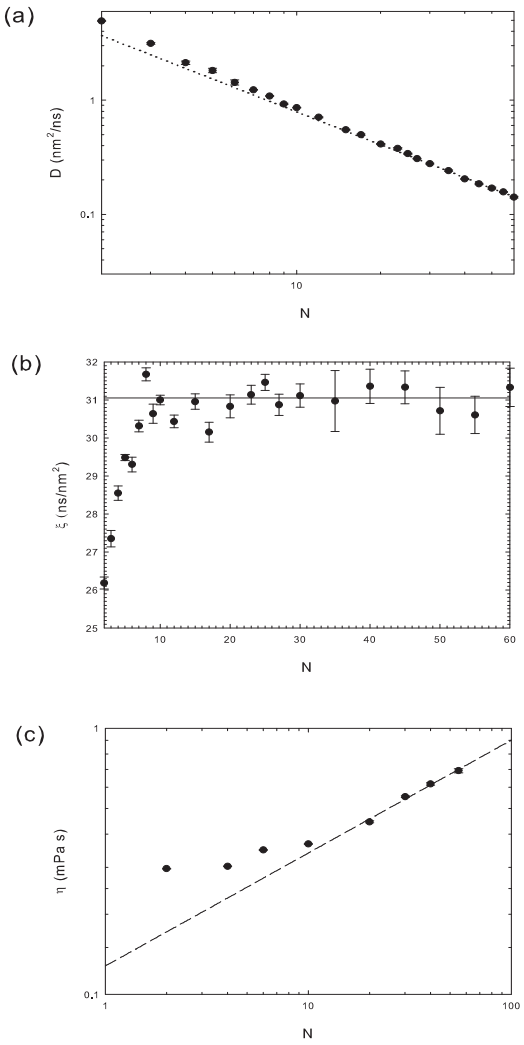

Fig. 2: (a) The COM self-diffusion coefficient D, (b) bead friction coefficient ξ and (c) viscosity η as a function of the chain length N for Model 3. The symbols represent simulation results, solid line denotes a constant value of ξ and dashed lines correspond to fit to $f(N) = A_0 N^{A_1}$; (a) $A_0 = 5.81_{113}$, $A_1 = -0.90_5$ and (c) $A_0 = 0.13_1$, $A_1 = 0.42_3$.

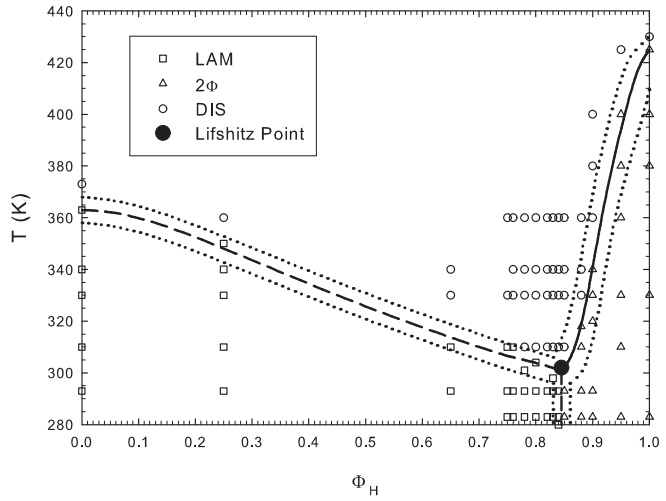

Fig. 5: The phase diagram along the $\Phi_H - T$ isopleth for $A_3/B_4/A_9$-B_9 model system that mimics the PDMS/PEE/PDMS-PEE melt. LAM, DIS and 2Φ denote the lamellar, disordered and two-phase regions, respectively. Dashed lines represent the phase boundaries between the regions and dotted line indicates the estimated uncertainties of the boundaries. Empty circles, squares and triangles represent simulation points.

in Fig. 5. The phase diagram thus exhibits three distinct regions: a high-temperature disordered region, a microphase-separated region with a lamellar phase, and a 2Φ macrophase-separated region. The Lifshitz point corresponding to the intersection between the line of disorder-lamellar transitions and the line of critical points is located at about $\Phi_H = 0.84 \pm 0.01$ and $T = 303 \pm 3$ K. In contrast to the experimental phase diagram that displays disordered, lamellar, BμE and multi-phase regions, the DPD phase diagram exhibits only disordered, lamellar, and 2Φ regions. The Lifshitz point for the model is located at concentrations corresponding to the narrow channel of BμE in the experimental phase diagram.

3.3 Diblock Copolymer-Homopolymers Systems

Under the order-disorder temperature, T_{OD}, the pure DBCs self-assemble into the four morphologies. Addition of homopolymers into DBC melts modifies the physical properties and the phase behavior of the pure DBC system, and consequently, it offers a relatively direct route to tailoring physical properties. For certain homopolymer concentrations the added homopolymers can induce morphological changes such as the transformation of a lamellar phase into a BμE [12]. Motivated by the rich phase diagram of the DBC-homopolymers systems we explored the phase behavior along a homopolymer volume fraction-temperature $\Phi_H - T$ isopleth for a ternary polymer melt consisting of two immiscible A and B homopolymers, and a symmetrical A-B DBC by DPD simulations. Our model ternary polymer system is intended to mimic a real ternary polymer melt of poly(diemthylsiloxane) (PDMS), poly(ethylethylene) (PEE) homopolymers and corresponding diblock copolymer (PDMS-PEE), i.e. PDMS/PEE/PDMS-PEE [45,46]. The polymer model parameters were derived using a top-down coarse-graining approach, applied to a PDMS/PEE/PDMS-PEE melt. The average molecular weights, M_p, were 2,130 g/mol, 1,770 g/mol, and 10,400 g/mol for PDMS, PEE, and PDMS-PEE, respectively, where the polydispersities were less than 1.1. PDMS and PEE were coarse-grained into chains with three and four mesoscopic beads, A_3 and B_4, respectively, while PDMS-PEE was coarse-grained into a symmetrical chain with 18 mesoscopic beads, A_9-B_9. Flory-Huggins interaction parameter χ_{AB} that in turn specifies the unlike interaction parameters, a_{AB}, was considered inversely proportional to temperature T as $\chi_{\mathrm{AB}} = A/T$ where A is an adjustable parameter related to the experimental $T_{OD} = 363$ K for the pure PDMS-PEE melt and to the experimental $T_C = 425$ K for the PDMS/PEE melt [45,46].

We were able to clearly distinguish between particular; disordered, lamellar and two phase (2Φ) states at all simulated state points. Plotting the simulation points on the $\Phi_H - T$ plane enables us to draw boundaries between the disordered and lamellar regions, between the disordered and 2Φ regions, and between the lamellar and 2Φ regions; i.e., to establish a phase diagram as displayed

3.2 Simulation Aspects of Lamellar Morphology

A finite volume of a simulation box together with the periodic boundary conditions can have a spurious effect on self-assembled morphologies of DBC systems [38–41]. If the box size is not commensurate with a thermodynamically stable structure, i.e., with a structure of the lowest free energy a mechanically stable structure can form instead or periodic spacing (e.g., lamellar width) can be altered. In the following, we systematically explored effects of the box size on DPD simulations of the lamellar morphology for pure DBCs. We performed DPD simulations in cubic boxes with $L^* = \{10, 11, ..., 40\}$. For each case, we ran 24 simulations that differ by initial seed for random number generator [42].

Fig. 3 displays mean lamellar spacing $\overline{W}^*$, averaged over all 24 runs and W^*_{pref}, the lamellar spacing with the highest number of observations within the set of 24 runs, for every L^*. Results are displayed for two relaxation scenarios (initial configuration and equilibration method) considered, i.e., INIT1 and INIT2. We see that the relaxation scenarios affect significantly values of $\overline{W}^*$ and only marginally values of W^*_{pref}. As shown below, averaging values of $\overline{W}^*$ over all L^* studied (dashed line in Fig. 3) does not lead to a value of W^*_n. Values of $\overline{W}^*$ for $L^* < 20$ are subject to large statistical uncertainties.

Then following Schultz et al. [43,44], we equalize the pressure in each direction by varying the box lengths at fixed system volume and find the natural lamellar spacing W_n, i.e., a lamellar width corresponding to a lamellar structure with the lowest free energy. This is demonstrated for system volume $V^* = 32^3$ and two lamellar orientations in Fig. 4. Here, we plot P^*_{xx}, P^*_{yy} and P^*_{zz} (Figs. 4a and 4d), P^*_{var} (Figs. 4b and 4e), and off-diagonal components of the pressure tensor P^*_{xy}, P^*_{xz} and P^*_{yz} (Figs. 4c and 4f), which become zero at W^*_n, as a function of $W^{*'}$. We see that the intersection of P^*_{xx}, P^*_{yy} and P^*_{zz} or minimum in P^*_{var} and/or intersection of P^*_{xy}, P^*_{xz} and P^*_{yz} clearly indicate the value of the natural lamellar spacing $W^*_n = 6.520_2$. The same value of W^*_n was also found for systems with different volumes, i.e., $V^* = \{20^3, 26^3, 39^3\}$ and different orientations of lamellar planes.

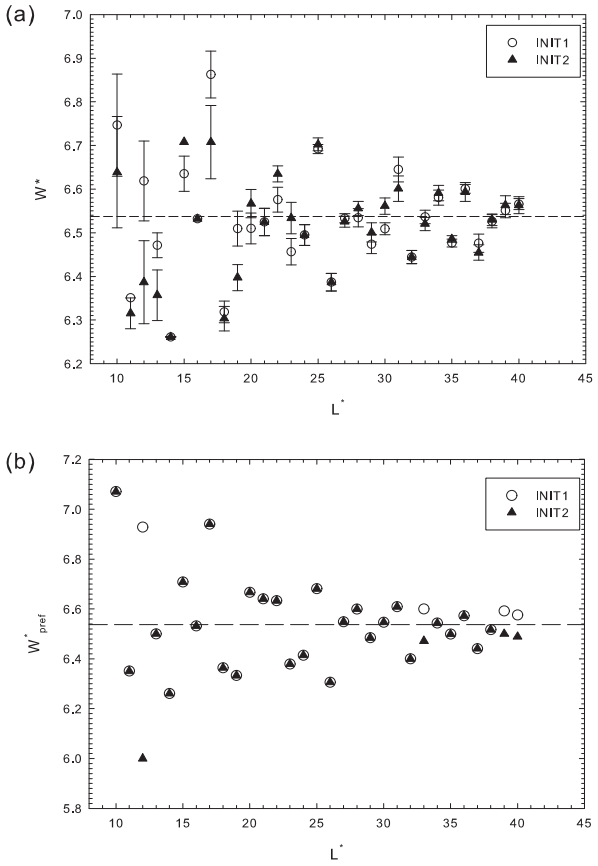

Fig. 3: (a) Lamellar spacing averaged over 24 independent DPD simulations, $\overline{W}^*$, and (b) preferential lamellar spacing, W^*_{pref}, as a function of the box length L^*, and relaxation scenarios (INIT1 and INIT2). The dashed line denotes an average over values of $\overline{W}^*$ for all L^* studied.

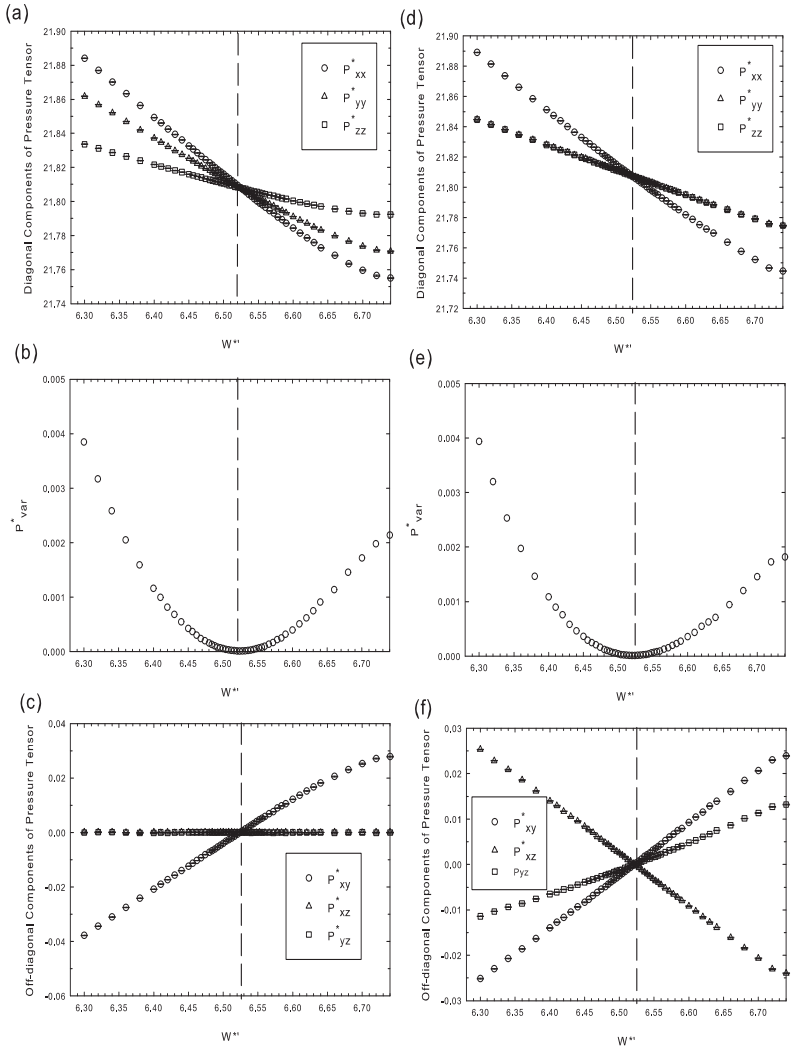

Fig. 4: (a,d) Diagonal components of the pressure tensor, (b,e) variance of diagonal components of the pressure tensor, P_{var}, and (c,f) off-diagonal components of the pressure tensor as a function of the lamellar spacing, $W^{*'}$, for cubic boxes with the volume $V^* = 32^3$. Left and right columns correspond to the lamellar orientation $\boldsymbol{n} = (n_x, n_y, 0)$ and $\boldsymbol{n} = (n_x, n_y, n_z)$, respectively. The dashed lines indicate the position of natural lamellar spacing W^*_n.